Hydrogen diffusion in the cubic Laves phase of $ZrFe_2$

Hydrogen diffusion in the cubic Laves phase of ZrFe$_2$

C U Maier† and H Kronmüller

Max-Planck-Institut für Metallforschung, Institut für Physik, D-7000 Stuttgart 80, Federal
Republic of Germany

Abstract. For the cubic Laves-phase compound ZrFe$_2$ the method of magnetic relaxation was applied in a study of low-temperature diffusion processes of hydrogen. Two relaxation maxima were observed at 82 K and 108 K with mean activation enthalpies of $Q=0.14$ eV and 0.23 eV and pre-exponential factors of $\tau_0=10^{-7}$ s and 4×10^{-10} s, respectively. The relaxation at 82 K is assigned to H jumps during hydride formation which happens in this temperature region. The relaxation at 108 K is related to an orientation after-effect in the absence of any interaction between hydrogen atoms. This relaxation is assigned to atomic jump processes of hydrogen between the preferentially occupied interstitial tetrahedral sites formed by two Fe and two Zr atoms. The activation parameters of the long-range diffusion ($Q_{\text{diff}}=0.38$ eV, $D_0=3\times10^{-8}$ m^2 s^{-1}) were determined by thermal degassing.

1. Introduction

According to the constitution diagram [1] the binary system Fe–Zr possesses an intermetallic Laves-phase compound ZrFe$_2$ with a cubic MgCu$_2$ C15 structure (figure 1). The homogeneity range of ZrFe$_2$ is markedly asymmetric with respect to the stoichiometric composition Zr$_{33}$Fe$_{67}$ and is extended from Zr$_{27}$Fe$_{73}$ to Zr$_{34}$Fe$_{66}$ [1]. There are eight ZrFe$_2$ formula units per simple cubic unit cell ($a_0=7.06$ Å [1]) in this structure. The larger Zr atoms ($r_{\text{Zr}}=1.6$ Å) occupy a cubic diamond lattice. Regular tetrahedra built of four smaller Fe atoms ($r_{\text{Fe}}=1.26$ Å) are centred at the fourfold-coordinated interstitial sites of the diamond structure. The arrangement of near neighbours around a Zr atom (figure 1) is composed by 12 Fe and 4 Zr atoms whereas different nearest-neighbour distances ($r_{\text{Fe}-\text{Fe}}=2.50$ Å, $r_{\text{Fe}-\text{Zr}}=2.93$ Å, $r_{\text{Fe}-\text{Fe}}=3.06$ Å [2]) occur.

Because of the technological and scientific interest, hydrogen in Laves-phase compounds has been studied very extensively [3–6]. In particular, research into hydride properties for solid-state hydrogen storage has been focussed on large absorption capacities which correspond to hydrogen-to-metal ratios (H/M) larger then 1. However in the ZrFe$_2$ cubic Laves phase at $T=298$ K and with $p=61\times10^5$ Pa, hydrogen forms a solid solution phase and the solubility is rather low, i.e. H/M<0.16 [4], thus suggesting the investigation of hydrogen relaxation processes at lower temperatures, where the interaction between H atoms can be neglected. As previously shown [7–9] a

† Present address: Universität Stuttgart, Institut für Physikalische Elektronik, Pfaffenwaldring 47, D-7000 Stuttgart 80, Federal Republic of Germany.
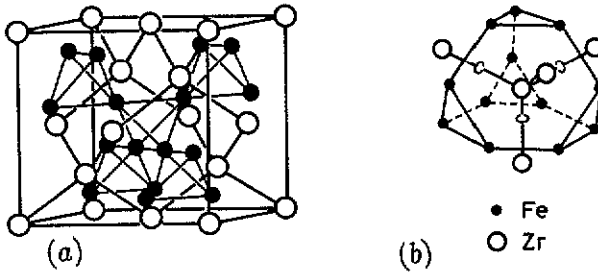
Figure 1. (*a*) Unit cell of a cubic Laves phase (C15 structure) and (*b*) the arrangement of nearest-neighbour atoms around a Zr atom.

very sensitive technique for studying the mobility of hydrogen in ferromagnetic alloys is based on the magnetic after-effect (MAE). The high sensitivity of MAE measurements allows us to detect H concentrations as low as 1 ppm. Furthermore, measurements at low temperatures are possible using this technique, since the orientation after-effect is sensitive with respect to one atomic jump per H atom.

In addition, the long-range diffusion of hydrogen in $ZrFe_2$ above room temperature is not influenced by hydride formation. A comparison between reorientations of H atoms measured by MAE and macroscopic diffusion processes determined by thermal degassing yields detailed information about the microstructure [10, 11] which determines the mobility of hydrogen.

2. Experimental details

2.1. Specimen preparation

The polycrystalline single-phase $ZrFe_2$ alloy was prepared by arc melting. The purity of the constituent transition metals was 99.9% (Zr) and RRR≈ 150 (Fe). To achieve a homogeneous single phase of this intermetallic compound an additional heat treatment at 1533 K for 24 h in HV was preformed. From this alloy parallelepipeds with a quadratic cross-section of $1.4 \times 1.4 \times 20$ mm^3 were produced. The stoichiometric composition of the $ZrFe_2$ specimens was 68.1 ± 1.4 at.% Fe and 31.9 ± 0.9 at.% Zr. Figure 2 shows a scanning microscopy photograph of a polished $ZrFe_2$ surface. The visible small dark areas deviate to about 1 at.% up to higher Fe concentration from the above-mentioned stoichiometry. No other intermetallic ZrFe phases were found. The crystalline structure was investigated by means of x-ray analysis in an angular range between 20° and 80°, using a monochromatic Cu Kα line ($\lambda = 0.154$ nm). Two dominating sharp reflexes at 42.4° and 64.5° were observed (figure 2) which can be identified as the (331) and (422) reflexes of the cubic Laves phase (C15 structure) of $ZrFe_2$ [12]. The grain size was around 100 μm. The $ZrFe_2$ specimens were H-charged in a H_2 atmosphere at T=1533 K under a pressure of 3×10^5 Pa.

2.2. Magnetic after-effect

The microscopic mechanism of magnetic after-effect [13] is based on the magnetic interaction energy between the directions of the spontaneous magnetization within
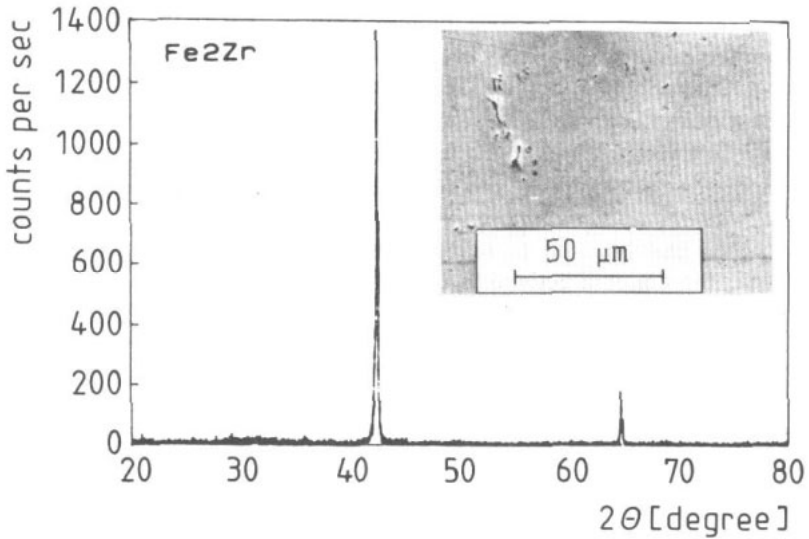
Figure 2. X-ray analysis and scanning microscopy photograph of a single-phase ZrFe$_2$ specimen.

a domain wall and the symmetry axis of anisotropic hydrogen interstitial configurations. Due to thermally activated jumps the reorientation of H atoms may lower this interaction energy leading to a decrease of the initial susceptibility, $\chi(t)$, i.e. the gradient of the initial magnetization curve. $\chi(t)$ is measured using an AC method [14], where a small oscillating pertubation of the magnetic field is applied. The analysis of the temperature-dependent H-induced relaxation processes yields the activation parameters [15]. Taking into consideration the reluctivity $r(t) = 1/\chi(t)$, isothermal relaxation curves are measured after each demagnetization of the specimen. The experimental results are represented as isochronal relaxation curves

$$\Delta r(t_1, t_2, T)/r(t_1, T) = [r(t_2, T) - r(t_1, T)]/r(t_1, T) \tag{1}$$

between the measurement times $t_1 = 0.5$ s and $t_2 = 1.5 - 179.5$ s. The ratio $\Delta r/r$ represents the relative reluctivity amplitude of the relaxation. Since $\chi(t)$ decreases with increasing time it follows that $r(t_2, T) > r(t_1, T)$ and $\Delta r/r$ corresponds to positive quantities.

The magnetic relaxation processes are described by a box-type distribution [16] of the activation enthalpy, where the relaxation times obey an Arrhenius law. In this case the time dependence of the reluctivity is given by

$$r(t, T) = r(0, T) + [r(\infty, T) - r(0, T)]G(t) \tag{2}$$

where the magnetic after-effect function, $G(t)$, is represented by

$$G(t) = 1 + [\mathrm{Ei}(-t/\tau_2) - \mathrm{Ei}(-t/\tau_1)]/\ln(\tau_2/\tau_1). \tag{3}$$

Ei denotes the exponential integral [17]. Fitting broad relaxation maxima, a superposition of more such box-type distributions is necessary for a satisfactory description.

2.3. Thermal degassing analysis

The H concentration and the diffusion kinetics of thermal H degassing were investigated by a manometric method [18]. The H-charged ZrFe$_2$ was thermally degassed at a constant heating rate, $\dot{T}$. The activation parameters Q_{diff} and D_0 were determined by using different $\dot{T_i}$ for each run. The temperature dependence of the degassing rate, dc/dt, was measured yielding characteristic maxima at T_i for each diffusion process. For $\dot{T_1} < \dot{T_2}$ a shift of the temperature, T_i, of the degassing maxima appears, which can be used to derive activation parameters. Assuming an Arrhenius behaviour, the discrete activation enthalpy, Q_{diff}, is given by

$$Q_{\text{diff}} = k \, \ln\left(\frac{\dot{T_2} \, T_1^2}{\dot{T_1} \, T_2^2}\right) \frac{T_2 T_1}{T_2 - T_1}. \tag{4}$$

For the determination of the pre-factor of the diffusion coefficient, D_0, the specimens, which are parallelepipeds of edge length L, were approximately described by cylinders with an effective radius, $\bar{r} = (L/4)(1 + \sqrt{2})$, which yields a pre-exponential factor D_0 given by [19]

$$D_0 = \left(\bar{r}/2.405\right)^2 \dot{T_i} \left(Q_{\text{diff}}/kT_i^2\right) \exp(Q_{\text{diff}}/kT_i) \tag{5}$$

where D_0 has the same value for each heating rate, $\dot{T_i}$, and the corresponding temperature of the degassing maximum, T_i. In the case of a possible surface impediment to the H desorption, the activation parameters of the degassing process have to be interpreted as effective values.

3. Results

3.1. Magnetic relaxations

After charging with H the ZrFe$_2$ specimen shows two overlapping relaxation maxima (figures 3 and 4). The maximum temperatures, T_{max}, and the relative amplitudes, $\Delta r/r$, were determined by splitting the fitted Q-spectrum (figure 4) and calculating separately each maximum with the same pre-exponential factor, τ_0. Therefore the MAE spectrum may be composed by two broadened maxima at around 82 K (0.14 eV) and 108 K (0.18 eV) with relaxation amplitudes of 47% and 16%, respectively.

   The isochronal annealing behaviour of the H-induced relaxation spectrum is shown in figure 3. After annealing at T_A=400 K the relaxation amplitudes decrease from 47% to 32% (82 K maximum) and from 16% to 11% (108 K maximum). At T_A=450 K a high degassing rate was observed and the 82 K maximum nearly disappeared whereas the 108 K maximum (figure 5) still shows a relative amplitude of 2.8% which leads to a change in the shape of the relaxation spectrum. At T_A=500 K no maxima appear, indicating a complete H degassing of the specimen.

   The relaxation spectra were fitted to exponential time laws of an orientation aftereffect (equation (2)) using ten superimposed box-type distributions [16, 20] of the activation enthalpy, $p(Q)$, and one pre-exponential factor, τ_0. Between T_A=280 K and 400 K a simultaneous numerical analysis of both maxima yields a common pre-factor $\tau_0 = 10^{-7 \pm 1}$ s and an average activation enthalpy of $\bar{Q}_{82\,\text{K}} = 0.14 \pm 0.03$ eV and $\bar{Q}_{108\,\text{K}} = 0.18 \pm 0.03$ eV, respectively. Due to the strong decrease of the
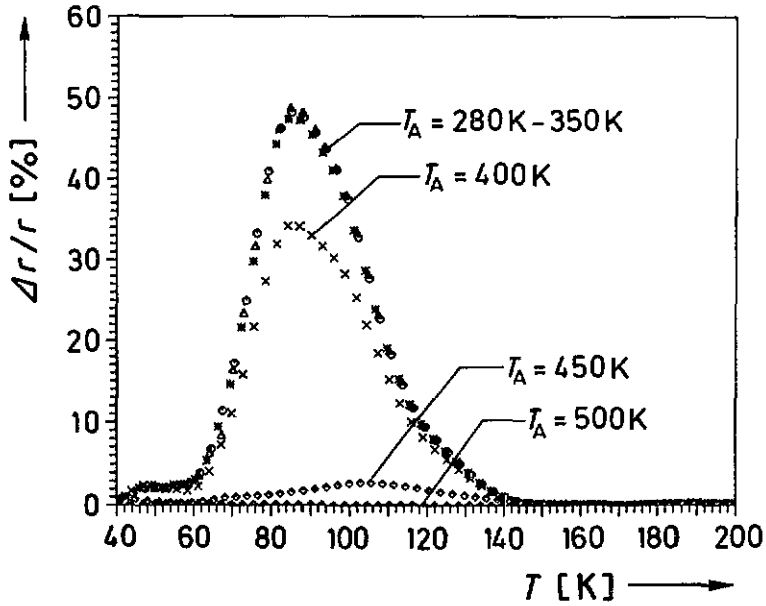
Figure 3. Isochronal relaxation spectra of H-charged $ZrFe_2$ at different annealing temperatures, T_A ($t_1 = 0.5$ s, $t_2 = 179.5$ s).
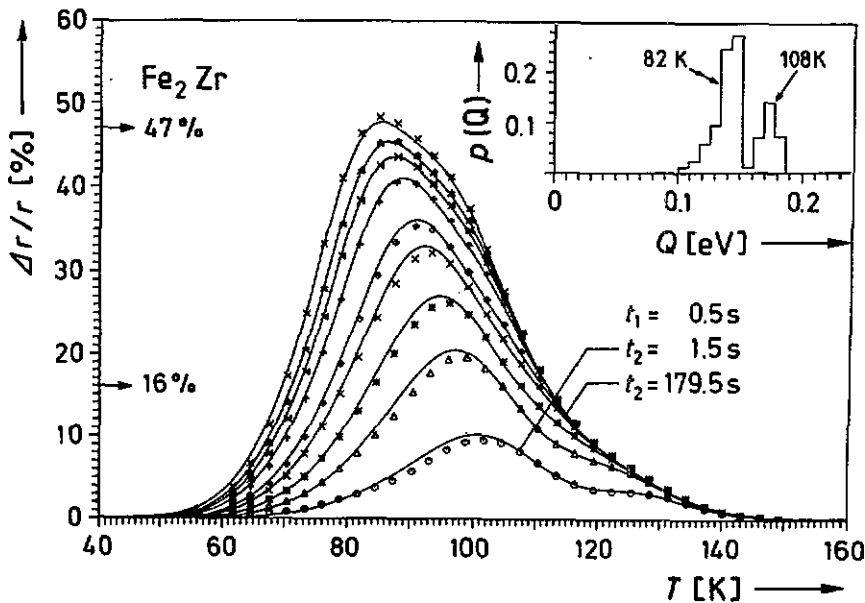

Figure 4. Relaxation spectrum of the H-charged $ZrFe_2$ alloy at $T_A = 300$ K. Experimental data are represented by symbols ($t_1 = 0.5$ s, $t_2 = 1.5$, 4.5, 9.5, 19.5, 29.5, 59.5, 89.5, 119.5, 179.5 s) and solid lines correspond to a numerical fit. The distribution of activation enthalpies, $p(Q)$, are shown within the spectra.

82 K maximum after $T_A = 450$ K the 108 K maximum could be fitted separately (figure 5) with $Q_{108 K} = 0.23 \pm 0.02$ eV and a distinctly lower pre-factor of $\tau_0 =$
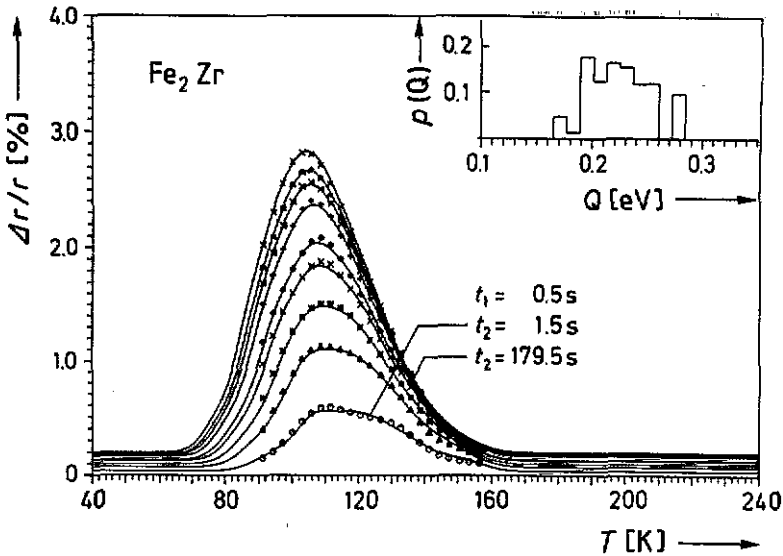
Figure 5. Numerical fit of the 108 K relaxation maximum of the H-charged ZrFe$_2$ alloy at T_A=450 K and the distribution of activation enthalpies, $p(Q)$, as in figure 4.

$4 \times 10^{-10\pm1}$ s. Because the H concentration is low, the interaction between H atoms can be neglected and the relaxation processes may be fitted by a sum of independent exponential functions. As demonstrated by figures 4 and 5 the fitting parameters used describe simultaneously the temperature shift, the half-width, and the amplitudes of the isochrones for varying measuring times, t_2. In general nine isochrones for different t_2 parameters have been fitted which is equivalent to nine different frequencies. The stability of the fit was reproduced within the given error range of the activation parameters and was therefore rather reliable.
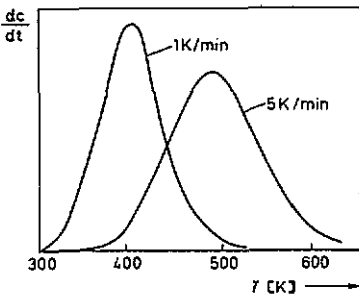

Figure 6. Degassing rate, dc/dt, of hydrogen in ZrFe$_2$ with heating rates of (a) 5 K min^{-1} and (b) 1 K min^{-1}.

3.2. Thermal degassing

The total H concentration of ZrFe$_2$ specimens was $c_H = (0.1 \pm 0.05)$ at.%. Figure 6 shows the temperature dependence of the degassing rate, dc/dt, at two different heating rates, $\dot{T}$=5 K min^{-1} and 0.5 K min^{-1}. The lower heating rate leads to a shift of the degassing maximum from T_{max}=494 K to 406 K due to the longer effective annealing time. According to equations (4) and (5) the activation parameters of the long-range diffusion are given by Q_{diff}=0.38±0.1 eV and $D_0 = 3 \times 10^{-8\pm2}$ m^2 s^{-1}.

3.3. Initial susceptibility of ZrFe₂

The initial susceptibility, $\chi(T)$, of H-charged ZrFe₂ (figure 7) measured at $t_2 =$ 1.5 s shows a plateau between 4.2 K and 40 K followed by a strong increase up to 85 K, indicating a possible magnetic or structural phase transition. Because the H concentration decreases with increasing T_A an increase of $\chi(T)$ is observed in the range between 85 K and 200 K. At $T = 320$ K, $\chi(T)$ reaches a maximum and decreases at higher temperatures. After annealing at 450 K, e.g., at low H concentrations, $\chi(T)$ is close to the curve for uncharged ZrFe₂. The plateau below 40 K increases to higher values and the H-induced drastic increase of $\chi(T)$ at 85 K disappears.
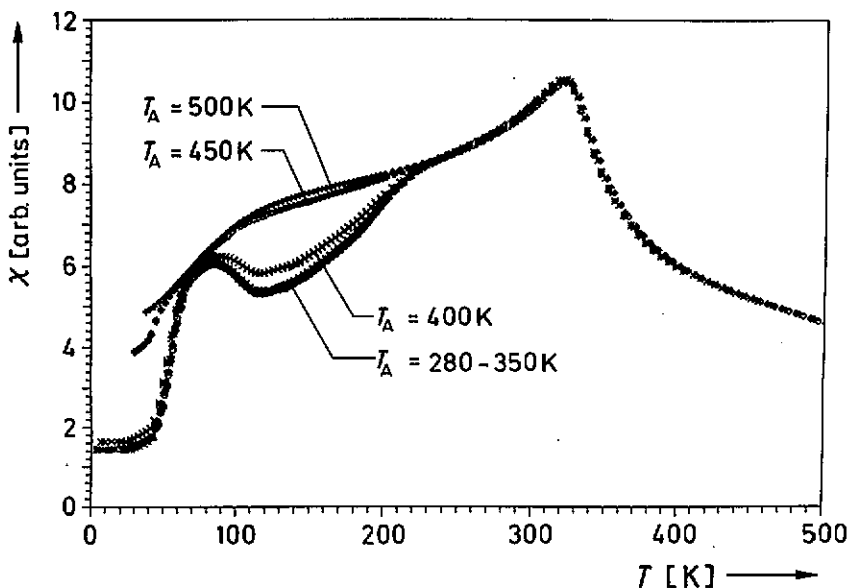

Figure 7. Annealing behaviour of the initial susceptibility, $\chi(T)$, in ZrFe₂ ($t_1 = 0.5$ s, $t_2 = 1.5$ s).

4. Discussion

4.1. Interpretation of the H relaxation processes

The H-induced overlapping maxima at 82 K and 108 K can be described in terms of reversible orientation after-effects, taking into account reorientations of H atoms between neighbouring anisotropic interstitial sites. The difference in the τ_0-values resulting from the simultaneous fit of both maxima ($10^{-7\pm1}$ s) and the separate numerical analysis of the 108 K maximum ($4 \times 10^{-10\pm1}$ s) indicates, that the larger pre-factor of 10^{-7} s is determined by the 82 K relaxation. A possible reason for this large τ_0-value could be the formation or dissolution of hydride phases within this temperature range. During such a phase transition the H atoms perform thermally activated jumps in the direction of H-rich hydride areas. Assuming Debye processes for the H jumps the corresponding relaxation times, $\tau_i(T)$, obey Arrhenius laws

$$\tau_i(T) = \tau_0 \exp(Q_i/kT). \tag{6}$$

The activation entropy, S, may be lowered, yielding a large pre-exponential factor τ_0 defined according to

$$\tau_0 = \tau_0^* \exp(-S/k) \tag{7}$$

where τ_0^* is the inverse of the attempt frequency, ν_0^*, of the hydrogen atom, which is independent of the entropy, S. In addition, the assignment of the 82 K relaxation to hydride formations is supported by the strong increase of $\chi(T)$ from 40 K to 90 K for higher H concentrations, which could be caused by the formation of hydride phases. These phases may be affected by additional pinning centres for the domain walls leading to a decrease of $\chi(T)$ below 90 K (figure 7). At low H concentrations ($T_A = 450$ K) the 82 K relaxation of the MAE spectrum disappears and no strong change of $\chi(T)$ around 80 K is observed indicating that no hydride precipitation occurs and, consequently, that the interaction between H atoms is small. On the basis of these results, the 82 K maximum is assigned to thermally activated H jumps during the formation of hydride phases.

The numerical analysis of the 108 K maximum yields a τ_0 in the range of typical pre-exponential factors for atomic hopping processes, $4 \times 10^{-10\pm1}$ s; this maximum is thus assigned to jumps of H atoms between neighbouring anisotropic interstitial sites in the cubic Laves phase $ZrFe_2$. These jumps are connected to a reorientation of the symmetry axes of the H configuration. Particularly at low H concentration hydrogen preferentially occupies the tetrahedral sites composed of two Fe and two Zr atoms (interstitial site A2B2; table 1) and the 108 K relaxation will be mainly determined by atomic H jumps between these neighbouring tetrahedral A2B2 positions. The jump processes of hydrogen at such low temperatures are assigned to tunnelling processes of H atoms from excited energy levels. In this model the jump frequency can be described by an Arrhenius law, where the temperature dependence of the relaxation frequency obeys equation (6). However, the pre-exponental factor is multiplied by the corresponding tunnelling probability [21] leading to an increase of τ_0.

Table 1. Tetrahedral interstitial sites in cubic Laves-phase compounds AB_2.

configuration	composition	number of sites per unit cell	next-neighbour configuration
B4	4B	8	4(AB3)
AB3	1A+3B	32	B4 + 3(A2B2)
A2B2	2A+2B	96	AB3 + 3(A2B2)

In recent NMR studies in similar cubic Laves phases [22, 23], e.g. TaV_2 and $ZrCr_2$, the activation parameters for the long-range H diffusion ($Q \approx 0.23$ eV, $\tau_0 \approx 10^{-12}$ s [22]) have been determined. In addition in these studies [22] a low-temperature relaxation process has been observed with unusual exponential temperature dependence. The values of the high-temperature relaxation process are closely comparable

to the present results and were also assigned to the hopping of hydrogen atoms between nearest-neighbouring interstitial sites of the type A2B2. This hopping mode is suggested to govern the long-range H diffusion also.

4.2. Atomic jump-rate model of H relaxation in cubic Laves-phase compounds

Three different types of tetrahedral interstitial position are available for the H atom in cubic Laves phases (table 1): one isotropic position (B4) and two anisotropic positions (AB3, A2B2). The numbers of these tetrahedral sites per unit cell and their nearest-neighbour interstitial sites are given in table 1. In spite of the 17 interstitial sites per formula unit (FU) only a maximal H occupation of slightly below 6 H atoms FU^{-1} was found ($ZrV_2H_{5.5}$ [4]). In general the H occupation in cubic Laves phases obeys the following rules.

   (i) *Chemical criteria.* If the component A (Zr) possesses a high H affinity in contrast to B (Fe), particularly at low H concentrations hydrogen preferentially occupies the tetrahedral sites containing the most A atoms (A2B2) [24].
   (ii) *Geometric criteria.* Nearest-neighbour tetrahedral sites cannot be occupied simultaneously. The minimal hole radius of the interstitial sites is $r_h = 0.40$ Å [25] and the minimal H–H distance is 2.1 Å (Westlake rules [6]).

The above criteria were confirmed by comparison of calculated local heats of formation of elementary (imaginary binary) hydrides [24] and neutron diffraction [26, 27] as well as time-differential perturbed angular correlation (TDPAC) measurements [28].
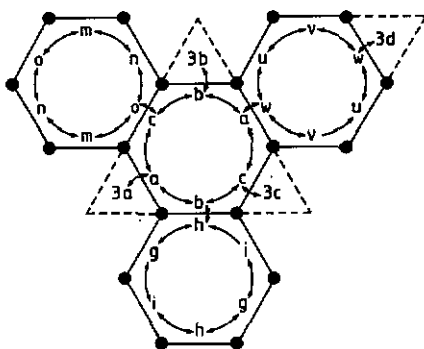

Figure 8. Two-dimensional representation of figure 1(*b*). The B atoms surrounding one A atom are shown in a projection. The energetically different interstitial tetrahedral sites in a ferromagnetic cubic Laves phase are noted for AB3 sites (3a, 3b, 3c, 3d) and A2B2 sites (a, b, c; g, h, i; m, n, o; u, v, w).

For the reorientation processes of hydrogen in ferromagnetic Laves phases (i.e., ZrFe$_2$)—using magnetic after-effect measurements—the atomic H jumps are induced by an energy of interaction between the anisotropy axis and the spontaneous magnetization [13]. This energy leads to a splitting of the anisotropic tetrahedral sites (AB3, A2B2) in four (AB3) and twelve (A2B2) energetically different sites per formula unit, respectively. Figure 8 shows a two-dimensional representation of the surrounding interstitial tetrahedral positions of one Zr (A) atom in the C15 structure. In the following the four AB3 sites are marked as 3a, 3b, 3c, 3d and the twelve A2B2 sites

as a, b, c, g, h, i, m, n, o, u, v, w. The change of the H concentration within one special tetrahedron may be given by rate equations. Considering only H jumps between nearest-neighbour sites we have to distinguish five different jump frequencies: ν_{13} (B4 → AB3), ν_{31} (AB3 → B4), ν_{32} (AB3 → A2B2), ν_{23} (A2B2 → AB3) and ν_{22} (A2B2 → A2B2). With this assumption, 17 coupled linear homogeneous differential equations of first order can be obtained

$$\partial c_1(t)/\partial t = -4\nu_{13}c_1 + \nu_{31}[c_{3a} + c_{3b} + c_{3c} + c_{3d}] \tag{8}$$

$$\partial c_{3a}(t)/\partial t = -(\nu_{31} + \nu_{32})c_{3a} + \nu_{13}c_1 + \nu_{23}[c_a + c_g + c_m] \tag{9}$$

$$\partial c_{3b}(t)/\partial t = -(\nu_{31} + \nu_{32})c_{3b} + \nu_{13}c_1 + \nu_{23}[c_b + c_n + c_u] \tag{10}$$

$$\partial c_{3c}(t)/\partial t = -(\nu_{31} + \nu_{32})c_{3c} + \nu_{13}c_1 + \nu_{23}[c_i + c_c + c_v] \tag{11}$$

$$\partial c_{3d}(t)/\partial t = -(\nu_{31} + \nu_{32})c_{3d} + \nu_{13}c_1 + \nu_{23}[c_o + c_h + c_w] \tag{12}$$

$$\partial c_a(t)/\partial t = -(\nu_{23} + \nu_{22})c_a + \nu_{32}c_{3a} + \nu_{22}[c_b + c_c + c_w] \tag{13}$$

$$\partial c_b(t)/\partial t = -(\nu_{23} + \nu_{22})c_b + \nu_{32}c_{3b} + \nu_{22}[c_a + c_c + c_h] \tag{14}$$

$$\partial c_c(t)/\partial t = -(\nu_{23} + \nu_{22})c_c + \nu_{32}c_{3c} + \nu_{22}[c_a + c_b + c_o] \tag{15}$$

$$\partial c_g(t)/\partial t = -(\nu_{23} + \nu_{22})c_g + \nu_{32}c_{3a} + \nu_{22}[c_h + c_i + c_u] \tag{16}$$

$$\partial c_h(t)/\partial t = -(\nu_{23} + \nu_{22})c_h + \nu_{32}c_{3d} + \nu_{22}[c_b + c_g + c_i] \tag{17}$$

$$\partial c_i(t)/\partial t = -(\nu_{23} + \nu_{22})c_i + \nu_{32}c_{3c} + \nu_{22}[c_h + c_g + c_n] \tag{18}$$

$$\partial c_m(t)/\partial t = -(\nu_{23} + \nu_{22})c_m + \nu_{32}c_{3a} + \nu_{22}[c_n + c_o + c_v] \tag{19}$$

$$\partial c_n(t)/\partial t = -(\nu_{23} + \nu_{22})c_n + \nu_{32}c_{3b} + \nu_{22}[c_m + c_n + c_c] \tag{20}$$

$$\partial c_o(t)/\partial t = -(\nu_{23} + \nu_{22})c_o + \nu_{32}c_{3d} + \nu_{22}[c_m + c_n + c_c] \tag{21}$$

$$\partial c_u(t)/\partial t = -(\nu_{23} + \nu_{22})c_u + \nu_{32}c_{3b} + \nu_{22}[c_v + c_w + c_g] \tag{22}$$

$$\partial c_v(t)/\partial t = -(\nu_{23} + \nu_{22})c_v + \nu_{32}c_{3c} + \nu_{22}[c_u + c_w + c_m] \tag{23}$$

$$\partial c_w(t)/\partial t = -(\nu_{23} + \nu_{22})c_w + \nu_{32}c_{3d} + \nu_{22}[c_u + c_v + c_a] \tag{24}$$

where $c_j(t)$ denotes the H concentration of the tetrahedral interstitial position j at time t.

Because of the preferential H occupation of the A2B2 sites at low H concentration, the orientation after-effect is assigned to H jumps between these anisotropic tetrahedral sites. Under this assumption the occupations and the corresponding jump frequencies of the B4 and AB3 sites are given by $c_1 = c_{3a} = c_{3b} = c_{3c} = c_{3d} = 0$ and $\nu_{ij} = 0$ ($i \neq j$), $\nu_{22} \neq 0$. Therefore the rate equations may be simplified to 12 coupled equations ((13)–(24)) depending only on ν_{22}, yielding the following relaxation frequencies:

$$\bar{\nu}_{1/2/3} = 5\nu_{22} \quad \text{(threefold degenerate)} \tag{25}$$

$$\bar{\nu}_{4/5/6} = 4\nu_{22} \quad \text{(threefold degenerate)} \tag{26}$$

$$\bar{\nu}_{7/8} = 3\nu_{22} \quad \text{(twofold degenerate)} \tag{27}$$

$$\bar{\nu}_{9/10/11} = \nu_{22} \quad \text{(threefold degenerate)} \tag{28}$$

$$\bar{\nu}_{12} = 0. \tag{29}$$

In this rate model the relaxation process of H atoms in the A2B2 sites of cubic Laves phases is described by four relaxation frequencies ((25)–(28)) which differ by at most a factor of 5.

For the H-charged $ZrFe_2$ specimen only the 108 K maximum could be assigned to H reorientation processes between the A2B2 sites. According to an Arrhenius law (equation (6)) the difference in the activation enthalphies, ΔQ, for the maximal deviation ($\bar{\nu}_{1/2/3} : \bar{\nu}_{9/10/11}=5$) is given by

$$\Delta Q = kT \ \ln(\tau_2/\tau_1) \qquad \tau_i \sim 1/\bar{\nu}_i. \tag{30}$$

For $T_{max}=108$ K the activation enthalpies are shown to be distributed over a range of $\Delta Q=15$ meV (equation (30)). Because these four relaxation processes are energetically similar, only one slightly broadened maximum is expected. This agrees with the MAE spectrum of the H-charged specimen where the characteristic maximum at 108 K appears. However, the observed enthalpy spectrum of the 108 K relaxation has the approximate value $\Delta Q=60$ meV and shows a distinctly broadened distribution which may be caused by dislocations and grain boundaries in the used polycrystalline $ZrFe_2$ specimen.

In conclusion, our analysis shows that the jump-rate model describes the measured 108 K relaxation maximum of the H-charged $ZrFe_2$ specimen and explains the observed broadened maximum which obeys the time law of an orientation after-effect.

4.3. Interpretation of the degassing spectra

From the small lattice constant of the $ZrFe_2$ unit cell ($a_0 = 7.06$ Å [1]), the hole radii of the A2B2, AB3, and B4 tetrahedral sites are 0.32 Å, 0.30 Å, and 0.25 Å [6], respectively. These values are distinctly smaller than the minimal radius ($r_h = 0.40$ Å) necessary for building stable hydrides at room temperature and this explains the small H absorption of 0.1 at.% in $ZrFe_2$. Furthermore, no stable hydride was found in $ZrFe_2$ above 290 K [29] and the observed degassing process of hydrogen in the temperature range investigated, between 300 K and 650 K, is not determined by the dissolution of a hydride and therefore is not correlated with the 82 K maximum.

The temperature position of the degassing maximum ($T_{max} = 406$ K for $\dot{T} = 0.5$ K min^{-1} (figure 6)) is nearly identical to the temperature where the maximal annealing rate of the 108 K maximum (410 K for $T \approx 0.5$ K min^{-1}) was observed. This agreement clearly shows that the long-range H diffusion and the magnetic reorientation after-effect of H atoms are governed by the same microscopic diffusion process. Therefore the degassing process may be assigned to a long-range H diffusion between the A2B2 tetrahedral sites, which are preferentially occupied in cubic Laves-phase compounds containing small H concentrations. Additionally only the A2B2 sites possess nearest neighbours of the same interstitial type A2B2 (table 1). Therefore the most probable diffusion paths are exclusively composed of these interstitial A2B2 sites and long-range H diffusion is determined by atomic H jumps between the anisotropic tetrahedral sites A2B2. In this case the activation parameters evaluated for the H-induced MAE relaxation, as well as for the degassing process of hydrogen, are expected to be equal, due to the microscopic jump processes being the same. Accordingly we should expect an activation enthalpy for H degassing, Q_{diff}, that is equal to the activation enthalpy for H jumps between neighbouring interstitial A2B2 sites, i.e. $Q_{diff} = 0.23$ eV. However, the H degassing process actually requires a transition of the H atoms through the grain boundaries as well as a desorption

from the specimen surface. Therefore the difference in the activation energies as measured for the degassing process ($Q_{diff} = 0.38 \pm 0.1$ eV) and for the atomic jump process between neighbouring A2B2 interstitial sites ($Q_{108\ K} = 0.23 \pm 0.02$ eV) may be attributed to the effect of grain boundaries or to additional desorption processes for hydrogen at the surface, where energetically high barriers lead to an increase of the activation enthalpy for the H degassing.

Acknowledgments

References

[1] Aubertin F, Gonser U, Campbell S J and Wagner H-G 1985 *Z. Metallk.* **76** 237
[2] Ennas G, Magini M, Padella F, Susini P, Buffitto G and Licheri G 1989 *J. Mater. Sci.* **24** 3053
[3] Shaltiel D 1980 *J. Less-Common Met.* **73** 329
[4] Shaltiel D, Jacob J and Davidov D 1977 *J. Less-Common Met.* **53** 117
[5] Ivey D G and Northwood D O 1986 *Z. Phys. Chem.* **147** 191
[6] Westlake D G 1983 *J. Less-Common Met.* **90** 251
[7] Kronmüller H, Higelin G, Vargas P and Lässer R 1985 *Z. Phys. Chem.* **143** 161
[8] Maier C U, Hirscher M and Kronmüller H 1989 *Phil. Mag.* B **60** 627
[9] Maier C U, Hirscher M and Kronmüller H 1991 *Phil. Mag.* B **63** 405
[10] Maier C U and Kronmüller H 1991 *J. Less-Common Met.* **172–174** 671
[11] Maier C U and Kronmüller H 1991 *Phys. Status Solidi* b **168** 425
[12] *International Centre of Diffraction Data* No 18-666
[13] Kronmüller H 1978 *Hydrogen in Metals I* ed G Alefeld and J Völkl (Berlin: Springer) p 289
[14] Walz F 1984 *Phys. Status Solidi* a **82** 179
[15] Hohler B and Kronmüller H 1982 *Phil. Mag.* **45** 607
[16] Richter G 1937 *Ann. Phys., Lpz.* **29** 605
[17] Abramowitz M and Stegun I A 1972 *Handbook of Mathematical Functions* (New York: National Bureau of Standards)
[18] Maier C U 1990 *Thesis* Universität Stuttgart
[19] Fromm E and Gebhardt E 1976 *Gase und Wasserstoff in Metallen* (Berlin: Springer)
[20] Cost J R 1983 *J. Appl. Phys.* **54** 2137
[21] Kronmüller H, Higelin G, Vargas P and Lässer R 1985 *Z. Phys. Chem.* **143** 161
[22] Skripov A V, Rychkova S V, Belyaev M Yu and Stepanov A P 1990 *J. Phys.: Condens. Matter* **2** 7195
[23] Skripov A V, Belyaev M Yu and Stepanov A P 1991 *Solid State Commun.* **78** 909
[24] Jacob I and Shaltiel D 1979 *J. Less-Common Met.* **65** 117
[25] Shoemaker D P and Shoemaker C B 1979 *J. Less-Common Met.* **68** 43
[26] Didisheim J J, Yvon K, Shaltiel D and Fischer P 1980 *J. Less-Common Met.* **73** 355
[27] Lynch J F, Johnson R and Reily J J 1979 *Z. Phys. Chem.* **117** 229
[28] Forker M, Herz W, Simon D and Lässer R 1989 *Z. Phys. Chem.* **164** 889
[29] Aubertin F, Gonser U and Campbell S J 1984 *J. Phys. F: Met. Phys.* **14** 2213